Class. Quantum Grav. **29** (2012) 184009 (11pp) doi:10.1088/0264-9381/29/18/184009

Exploring the WEP with a pulsed cold beam of antihydrogen

M Doser[1], C Amsler[2], A Belov[3], G Bonomi[4], P Bräunig[5], J Bremer[1], R Brusa[6], G Burkhart[1], L Cabaret[7], C Canali[2], F Castelli[8], K Chlouba[9], S Cialdi[8], D Comparat[7], G Consolati[10], L Di Noto[6], A Donzella[4], A Dudarev[1], T Eisel[1], R Ferragut[10], G Ferrari[11], A Fontana[12], P Genova[13], M Giammarchi[14], A Gligorova[15], S Gninenko[3], S Haider[1], J P Hansen[15], S Hogan[16], L Jorgensen[1], T Kaltenbacher[1], A Kellerbauer[17], D Krasnicky[18], V Lagomarsino[18], S Mariazzi[19], V Matveev[3], F Merkt[16], F Moia[10], G Nebbia[20], P Nedelec[21], M Oberthaler[5], D Perini[1], V Petracek[9], F Prelz[14], M Prevedelli[22], C Regenfus[2], C Riccardi[13], O Rohne[23], A Rotondi[13], M Sacerdoti[14], H Sandaker[15], M Spacek[9], J Storey[2], G Testera[24], A Tokareva[3], D Trezzi[14], R Vaccarone[24], F Villa[8], Z Zavatarelli[24] and A Zenoni[4] (AEGIS Collaboration)

[1] Physics Department, European Organisation for Nuclear Research, 1211 Genève 23, Switzerland
[2] Physics Institute, University of Zurich, Winterthurerstrasse 190, 8057 Zürich, Switzerland
[3] Institute for Nuclear Research of the Russian Academy of Sciences, 7a 60th October Anniversary Prospect, Moscow 117312, Russia
[4] Department of Mechanical and Industrial Engineering, University of Brescia, Via Branze 38, 25133 Brescia, Italy
[5] Kirchhoff Institute for Physics, University of Heidelberg, Im Neuenheimer Feld 227, 69120 Heidelberg, Germany
[6] Department of Physics, University of Trento, Via Sommarive 14, 38050 Povo (Trento), Italy
[7] Centre National de la Recherche Scientifique, Laboratoire Aimé Cotton, Campus dOrsay, 91405 Orsay Cedex, France
[8] Department of Physics, University of Milano, Via Celoria 16, 20133 Milano, Italy
[9] Department of Physics, Czech Technical University in Prague, Brehová 7, 115 19 Praha 1, Czech Republic
[10] Department of Physics, Politecnico di Milano, Piazza Leonardo da Vinci 32, 20133 Milano, Italy
[11] Istituto Nazionale di Ottica, Consiglio Nazionale delle Ricerche, Largo Fermi 6, 50125 Firenze, Italy
[12] Istituto Nazionale di Fisica Nucleare, Sezione di Pavia, Via Agostino Bassi 6, 27100 Pavia, Italy
[13] Department of Nuclear and Theoretical Physics, University of Pavia, Via Agostino Bassi 6, 27100 Pavia, Italy
[14] Istituto Nazionale di Fisica Nucleare, Sezione di Milano, Via Celoria 16, 20133 Milano, Italy
[15] Institute of Physics and Technology, University of Bergen, Alleegaten 55, 5007 Bergen, Norway
[16] Laboratory for Physical Chemistry, ETH Zurich, 8093 Zürich, Switzerland
[17] Max Planck Institute for Nuclear Physics, Saupfercheckweg 1, 69117 Heidelberg, Germany
[18] Department of Physics, University of Genova, Via Dodecaneso 33, 16146 Genova, Italy
[19] Istituto Nazionale di Fisica Nucleare, Gruppo collegato di Trento, Via Sommarive 14, 38050 Povo (Trento), Italy
[20] Istituto Nazionale di Fisica Nucleare, Sezione di Padova, Via Marzolo 8, 35131 Padova, Italy
[21] Institut de Physique Nucléaire de Lyon, Claude Bernard University Lyon 1, 4 Rue Enrico Fermi, 69622 Villeurbanne Cedex, France
[22] Department of Physics, University of Bologna, Via Irnerio 46, 40126 Bologna, Italy

[23] Department of Physics, University of Oslo, Sem Slands vei 24, 0371 Oslo, Norway
[24] Istituto Nazionale di Fisica Nucleare, Sezione di Genova, Via Dodecaneso 33, 16146 Genova, Italy

E-mail: michael.doser@cern.ch

Received 1 February 2012, in final form 13 May 2012
Published 15 August 2012
Online at stacks.iop.org/CQG/29/184009

Abstract
The AEGIS experiment, currently being set up at the Antiproton Decelerator at CERN, has the objective of studying the free fall of antimatter in the Earth's gravitational field by means of a pulsed cold atomic beam of antihydrogen atoms. Both duration of free fall and vertical displacement of the horizontally emitted atoms will be measured, allowing a first test of the WEP with antimatter.

PACS numbers: 04.80.−y, 07.77.Gx, 07.60.Ly, 32.80.Ee, 32.80.Rm, 36.10.−k, 36.10.Dr, 37.25.+k, 82.45.Aa, 82.45.Yz

(Some figures may appear in colour only in the online journal)

1. Introduction

The primary scientific goal of the AEGIS experiment [1] is the direct measurement of the Earth's local gravitational acceleration g on antihydrogen ($\bar{H}$). The weak equivalence principle, which postulates that the behavior of a body in an external gravitational field should not be affected by its composition, has been extensively tested with ordinary matter. However, a number of attempts to formulate quantum theories of gravity, or to unify gravity with the other forces [2] lead to the possibility of a non-identical gravitational interaction between matter and antimatter. Furthermore, to date, it has not been possible to directly search for any such differences with antimatter, due to overwhelming systematic effects. Thus, even a measurement with a initially modest precision is scientifically relevant, as it will represent the first direct measurement of the gravitational interaction between a matter and an antimatter system.

In a first phase of the experiment, a gravity measurement with 1% relative precision will be carried out by observing the vertical displacement (using a high-resolution position-sensitive detector) of the shadow image produced by the passage of an an $\bar{H}$ beam through a Moiré deflectometer, the classical counterpart of a matter wave interferometer. This measurement requires pulsed production of $\bar{H}$ atoms in order to measure—in addition to the vertical displacement—the time of flight of each atom. Furthermore, the ensemble of formed atoms needs to be cold in order to minimize the beam divergence once they are accelerated, and thus the required measurement time. Estimating the initially achievable precision requires understanding the efficiencies of the different steps, as well as their uncertainties, and these have been quantified through direct measurements and the calculations and simulations that are detailed below.

The apparatus has been designed in such a manner that investigation of a number of further physics topics, either directly related to the primary goal detailed above, or completely

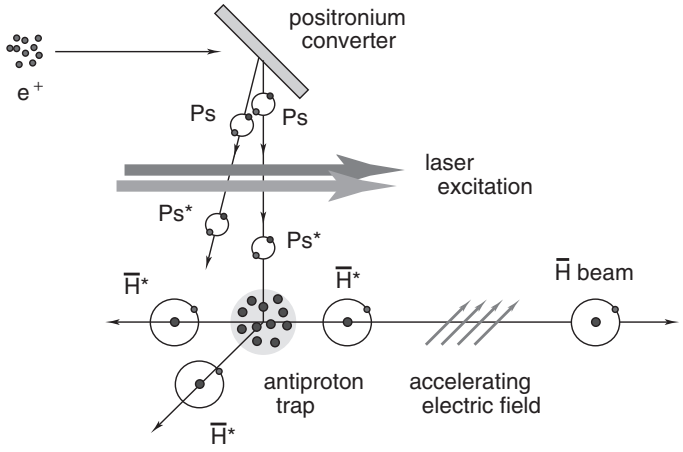

Figure 1. Proposed method for the production of a pulsed beam of cold $\bar{H}$ atoms.

independent, can be carried out as well. In particular, efforts leading to manipulations and trapping of Rydberg antihydrogen have the potential to lead to much higher sensitivity tests of the WEP with antimatter in the longer term.

2. Steps toward an antihydrogen beam

The essential steps leading to the production of a pulsed cold beam of $\bar{H}$ and the measurement of g with AEGIS are the following (figure 1).

- Production of positrons (e^+) from a Surko-type source and accumulator.
- Capture and accumulation of $\bar{p}$ from the AD in a cylindrical Penning trap.
- Cooling of the $\bar{p}$ to sub-K temperatures.
- Production of positronium (Ps) by bombardment of a cryogenic nanoporous material with an intense e^+ pulse.
- Excitation of the Ps to a Rydberg state with principal quantum number $n \sim 20$.
- Formation of $\bar{H}$ by resonant charge exchange between Rydberg Ps and cold $\bar{p}$.
- Pulsed formation of an $\bar{H}$ beam by Stark acceleration with inhomogeneous electric fields.
- Determination of g in a two-grating Moiré deflectometer coupled with a position-sensitive detector.

The feasibility of the different steps have either been conclusively demonstrated (e.g. by the ATHENA, ATRAP and ALPHA collaborations (see, in particular, [3, 4])), or are based on reasonable extrapolations of known results or calculations, which however remain to be validated. The steps and numbers leading to the expected resolution, as well as the effect of possible systematic errors, will be discussed in the following.

The experimental apparatus which realizes the different steps consists of

- a positron source (50 mCi) and accumulator,
- a high-field magnet (5T) housing trapping electrodes designed to maximize the antiproton trapping efficiency.
- a separate low-field highly homogeneous magnet (1T) which houses the antihydrogen production and beam formation structures.

- a cryogenically-housed Moiré deflectometer consisting of two 150-mm gratings placed at 1 m and 1.5 m from the antihydrogen formation point, along with a high-resolution antihydrogen detector at 2 m.
- A laser system that implements a Ps excitation scheme to a Rydberg state that foresees passing through an intermediate state ($n = 3$). An optional extension will investigate the alternative of passing through $n = 2$.

2.1. Trapping of antiprotons and accumulation of positrons

Antiprotons extracted from the Antiproton Decelerator (AD) at CERN at 100 MeV/c are degraded further by passing through a foil with tunable thickness. Simulations using Geant 4 [5] taking into account the beam characteristics, the beam optics, the multiple scattering and annihilation in the degrading foils, and the geometry and magnetic field of the 5 T magnet which houses the trapping electrodes have been used to optimize the overall trapping efficiency. A critical element is not only the field strength of the magnet, but also the depth of the trapping potential. The design and fabrication of the high voltage electrodes and of the attached electronics was carried out with particular care to ensure that trapping voltages of up to 20 kV are possible. This in turn is expected to allow trapping up to 0.1% of the incoming $\sim 3 \times 10^7$ antiprotons with a broad energy distribution after the degrader [6]. These $\sim 3 \times 10^4$ trapped antiprotons are cooled by interaction with electrons that in turn are cooled through their synchrotron radiation in the cryogenic bore of the 5 T magnet. Based on past experience, losses during this cooling procedure are expected to be small; similarly, transfer of the cooled antiprotons into the 1T magnet is expected to be very efficient. The duty cycle of the AD ($\sim$100 s) determines the overall accumulation rate of antiprotons, should stacking of several pulses be necessary to reach 10^5 trapped antiprotons. This trapping rate should increase by approximately two orders of magnitude once the ELENA decelerator, planned for commissioning in 2016, is operational.

Positrons will be accumulated using a two-stage Surko-type positron accumulator [7]. The operation of the positron accumulator is based on buffer gas capture and cooling of positrons in a Penning–Malmberg trap. Positrons emitted from a radioactive ^{22}Na source are moderated using solid neon. Moderators are usually grown at a temperature of 7 K with ultra-pure neon admitted at a pressure of 10^{-4} mbar for a few minutes. After the moderator a slow positron beam with typically 2×10^5 positrons/s mCi is obtained. Using a 50 mCi source $10^7 e^+$/s are expected. The accumulator traps and cools this continuous beam of slow positrons guided into the trapping region using axial magnetic field transport. Standard non-neutral plasma manipulation techniques (rotating wall) are used to radially compress the positron cloud, thus increasing the storage time and the number of accumulated positrons, which should reach $\sim 10^9$ within a duty cycle of the AD with a somewhat stronger source (to be installed in 2014) and moderate improvements in the trapping efficiency.

2.2. Formation of Ps

Positronium will be obtained in AEGIS by sending a pulse of positrons on a suitable target acting as positronium converter with high efficiency. Positronium formation in porous materials [8] is particularly suitable: Ps formed in the bulk can diffuse into a pore or can be formed at the surface of the pore. If the pores are connected to the surface of the material, the positronium can escape from the target toward the surrounding vacuum by following the pore channels and colliding with the pore walls, thermalizing in the process. The energy spectrum of the emitted positronium depends on the energy of the positronium entering the pore, on the number of

collisions with a pore surface and on the mean energy loss for each collision. The depth in the bulk where positronium is formed depends on the e^+ implantation energy (O(10 keV)) and with an appropriate choice of material (such as Xerogel [11]) or design (such as in [12]) of the pore geometry and of the implantation energy, we expect to be able to tailor the energy spectrum of the emitted positronium to match the required values (see section 2.4).

Because of the desirability of low temperature antihydrogen and of minimizing the distance between the target and the ultra-cold antiprotons, the target will be enclosed in the sub-K antihydrogen production region, and will thus itself lie at cryogenic temperatures. A quantum mechanical treatment (Ps scattering on phonons in potential wells) is required to predict the thermalization of positronium in nanopores at low temperature. Brusa *et al* [9] have shown that the minimum temperature that Ps atoms reach in a potential well (nanopore) is determined by the well (pore) dimensions: for pore dimensions smaller than a few nanometers single-phonon scattering does not allow to reach the ground state. Increasing the diameter of the nanochannels decreases the minimum accessible temperature: in nanostructures of 20 nm, it is around 7 K. On the other hand, an increase in the diameter of nanochannels is expected to extend the thermalization time of ortho-positronium (o-Ps) due to a reduction in the collisional frequency with the pore walls [9]. It is thus necessary to optimize the nanochannel dimensions to reach the optimal o-Ps temperature that maximizes the antihydrogen formation rate. Up to 40% of the injected positrons produce o-Ps; at the appropriate injection energies (several keV), about 20% of the Ps diffuse out of the target for a total of 3% of *thermalized* o-Ps at room temperature [10, 12]. These expected $\sim 10^7$ thermalized o-Ps emitted from the target are currently assumed to be emitted isotropically. However, quantum effects within the narrow pores produce a lower bound on the minimal temperature in the transverse plane to the pore axis, while the component parallel to the axis is unbounded, resulting in anisotropic cooling. The velocity component perpendicular to the pore axis is thus expected to dominate over the parallel component [9], which would lead to preferential directional emission.

2.3. Laser-excitation of o-Ps

Antihydrogen production by charge exchange between positronium atoms and antiprotons requires efficient excitation of positronium atoms up to high-n levels (Rydberg levels). The two lasers for a two-step incoherent optical excitation, $1 \rightarrow 3 \rightarrow n$ [13] have been constructed and will be optimized with positronium produced both inside the AEGIS magnet as well as on an external test platform. The rationale for choosing this scheme, rather than the alternative $1 \rightarrow 2 \rightarrow n$ scheme is (i) that the $n = 3$ state has a longer lifetime of 10.5 ns than the $n = 2$ state (with 3 ns), (ii) that the laser energy per pulse required to saturate the transitions is lower, an important consideration when losses into the cryogenic environment of the experiment must be minimized and (iii) calculations of the excitation efficiency [14] indicate a higher value when passing through the $n = 3$ level.

The Ps atoms are emitted from a cryogenic surface, although their temperature should be substantially higher. We aim at an effective temperature of 100 K, corresponding to a velocity of $\sim 3 \times 10^4$ m s^{-1}. The Ps atoms move in a relatively strong magnetic field of 1 T. In these conditions the combination of the Doppler, motional Stark, linear and quadratic Zeeman effects results in a broadening of the (second) excitation transition frequencies of the order of 1 THz, making the excitation process substantially less selective than in the usual case of Rydberg spectroscopy. Furthermore, the laser pulse length is required to be of few ns, and to have maximal overlap with an expanding cloud with an initial transverse area of ~ 6 mm^2. The requirements on the energy and bandwidth of the excitation laser suggest the use of optical parametric generation and amplification technology for both wavelengths. The laser

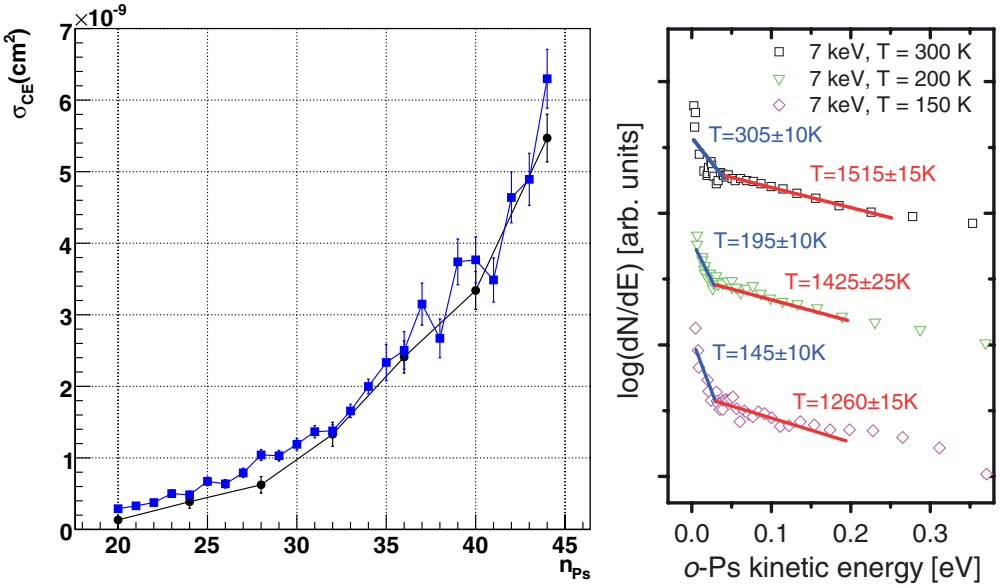

Figure 2. (Left) Cross section for the formation of Rydberg antihydrogen through the charge exchange process $\bar{p} + \mathrm{Ps}^* \rightarrow \bar{H}^* + \mathrm{e}^-$ as a function of n_{Ps} (the Ps* principal quantum number) for Ps* with a velocity ratio k_v of 1, and two assumptions on l_{Ps^*}: squares refer to l_{Ps^*} randomly chosen between 0 and $n_{\mathrm{Ps}} - 1$ while circles correspond to $l_{\mathrm{Ps}^*} = 2$. (Right) *o*-Ps energy spectra for different Ps production target temperatures (from [10]). The $\bar{H}$ formation cross section is greatest for $k_v \leqslant 1$, equivalent to Ps* temperatures $O(100\ \mathrm{K})$ for $n_{\mathrm{Ps}} \sim 30$.

system is composed of two subsystems: one for the generation of 205 nm radiation and the other for the generation of [1650–1700] nm radiation, both driven by a Q-switched Nd:YAG laser delivering a maximum of 650 mJ in 4 ∼6 ns pulses. The width of the first transition is determined by the Doppler width of the emitted *o*-Ps cloud (32 GHz at 100 K), while the width of the second transition is dominated by the motional Stark effect (∼THz). The laser systems have enough power to guarantee a 30% transition efficiency. The completed and tested system can cover a frequency band wide enough to excite different Rydberg levels (from $n = 16$ to the ionization limit), and exceeds the saturation power by more than a factor of 10 for both transitions, maintaining a great flexibility for the choice of the best strategy for obtaining a large number of antihydrogen atoms. An alternative laser excitation route (first to the $2\ ^3P$ state, and subsequently to $n = 10 \sim 25$) has recently demonstrated high efficiency production of Rydberg positronium, even in magnetic fields [15]. However, this study also emphasizes that already in relatively weak magnetic fields (0.16 T), the motional Stark effect may limit the achievable Rydberg states to $n \leqslant 20$.

2.4. Formation of antihydrogen

Antihydrogen atoms are formed by the charge exchange process $\bar{p} + Ps^* \rightarrow \bar{H}^* + \mathrm{e}^-$. The cross section for this process has been evaluated through Classical Trajectory Monte Carlo (CTMC) simulations [1], which indicate—as expected—a strong dependence of the cross section on the principal quantum number of the Rydberg positronium, and on the relative velocity of the antiprotons and of the Ps* (or more precisely, on the ratio k_v of the relative velocity between the positronium and the antiproton, v_r, and the Rydberg positronium internal motion, v_{orb}). Figure 2 shows the production cross section as a function of the Ps* principal quantum number.

While optimization of this parameter to maximize the antihydrogen production rate is possible by changing the wavelength of the second laser, the precise behavior of Rydberg atoms in the strong-field regime and in crossed $E \times B$ fields has not yet been thoroughly investigated. In particular, calculations and simulations of highly excited hydrogen atoms [16] indicate that the electric-field gradient required in the subsequent acceleration of Rydberg antihydrogen atoms (see subsection 2.5) will be rather limited, among others because of sub-level crossings and the possibility of field ionization.

The emission velocity of Ps from a nanoporous target as in section 2.2 is determined by the target temperature, the interaction time of the Ps inside the target (which is itself a function of the injection energy of the positrons into the target and the topology of the target material), and by the pore size. The first two aspects have been investigated in [17] which shows that for specific target compositions, the velocity distribution of *o*-Ps emitted from the target surface shows evidence of (partial) thermalization. Of particular interest in the case of AEGIS is the behavior at cryogenic temperatures. Recent first studies [10] have shown that the temperatures both of the thermalized component, but also of the only partially thermalized component of *o*-Ps, follow a decrease in the target temperature (figure 2). A lower bound on the *o*-Ps temperature is given by the dimensions of the pores [9]. While it is difficult to determine precisely the degree to which the two parameters affecting the Rydberg antihydrogen production rate can be optimized, an estimate can be obtained by assuming that the currently observed fraction of Ps* with a velocity component between 5 and 15 km s^{-1} (in which the the CTMC-derived cross section is approximately constant and $O(10^{-9}\ cm^2)$) is maintained also at cryogenic temperatures, and that a principal quantum number $n = 30$ can be achieved (the cross section is a factor of 5 lower in the case of $n = 20$). With 10^5 antiprotons, and the assumption of isotropic emission of *o*-Ps from the production target positioned at a distance of 15 mm, 10–100 Rydberg antihydrogen atoms should be produced in a pulse of several ns.

Achieving a sufficiently cold cloud of antiprotons is a central requirement of the experiment; the target antiproton temperature of 100 mK requires thermalizing the electrodes (which form the harmonic well in which the antiprotons will be held before interacting with the excited positronium) to the temperature of a dilution refrigerator (50 mK), while at the same time ensuring electrical insulation. Thermal coupling of the antiprotons to the surface temperature of the electrodes will be done by embedding the antiprotons in a cloud of electrons, and coupling these to the electrodes via dissipative circuits. Electrons present in the environment of antiprotons should not affect the pulsed formation (with a timescale of $\sim$10 ns) and acceleration (with a timescale of $\sim$10 μs) of antihydrogen; furthermore, requiring that the (electron plasma density dependent) rotation velocity of the electron plasma does not exceed that of a thermal distribution at 100 mK limits the number of electrons that can be used to cool the antiprotons to $\sim 10^5$ [1], further reducing the likelihood that any formed Rydberg antihydrogen may interact with the electrons that are present. The degree to which sufficiently low temperatures can be reached in this manner is an experimental question, which will be investigated in the coming years with protons and antiprotons, where also further cooling techniques, such as evaporative [18] or adiabatic [19] cooling will be attempted. Alternatively, antiprotons could be cooled sympathetically by interactions with laser-cooled atomic anions [20], potentially allowing to cool antiprotons to μK. A dedicated experiment to investigate this possibility has been set up and is systematically exploring the structure of potential negative ions in view of establishing the feasibility of this scheme. A first negative ion species, Os^-, has been thoroughly investigated [21, 22], but only partially meets the requirements for *efficient* laser cooling due to the rather low transition rate, which would require pre-cooling the antiprotons to $\sim$K temperatures. The design of the injection region of the apparatus (upstream of the 5 T magnet) incorporates the option for injecting negative ions from an external source,

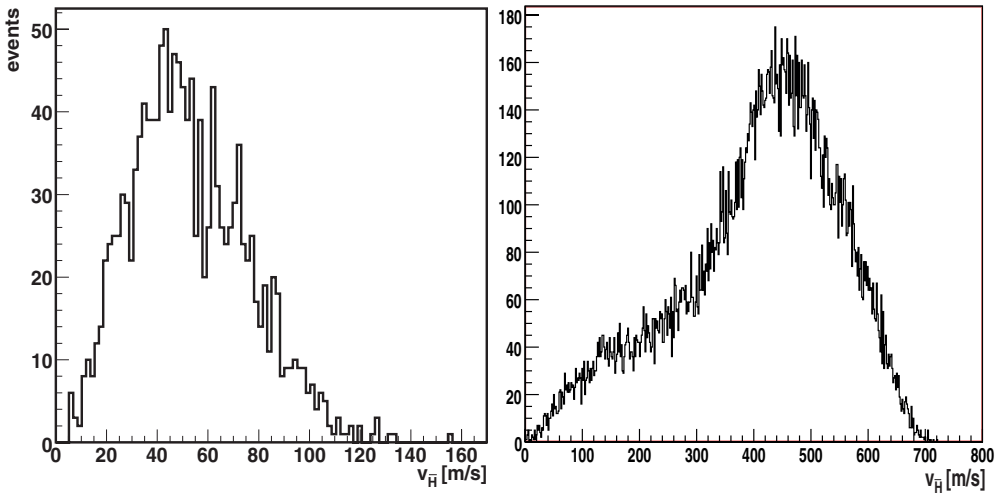

Figure 3. (Left) Antihydrogen velocity distribution from a CTMC simulation obtained for 100 mK antiprotons and $n_{Ps} = 35$ with $k_v = 1$. (Right) Horizontal velocity distribution of a Stark-accelerated antihydrogen beam obtained by accelerating $n = 30$ (rms = 4) antihydrogen Rydberg states (CTMC simulation).

for which space has been reserved on the upstream side of the apparatus. Similarly, the design of the electrodes holding antiprotons, as well as of the central region between the 1 T and the 5 T magnets, incorporates the option for injecting the required laser light to optically cool any negative ions, if an appropriate species can be identified.

2.5. Acceleration of antihydrogen

The Rydberg antihydrogen atoms will be axially accelerated through their coupling to an externally applied pulsed electric-field gradient (Stark acceleration), applying techniques proposed for and demonstrated with Rydberg hydrogen atoms [23], wherein atoms moving with an initial velocity of ∼700 m s^{-1} are stopped in a few μs over a distance of 2 mm. In the case of AEGIS, the inhomogeneous electric field is applied by appropriately polarizing the electrodes that initially confine the ultra-cold antiprotons immediately after the pulsed formation of antihydrogen (figure 4). Although the quantum numbers of the Ps* used to form Rydberg antihydrogen are fairly well determined by the laser excitations (although the magnetic sublevels are randomly populated), the charge exchange process will populate a range of (n, m, l) antihydrogen states. It should also be pointed out that these are no longer good quantum numbers in the $E \times B$ fields that appear at the moment of applying an electric-field gradient. Instead, our simulations use the (n, k) quantum numbers (where $k = n_1 - n_2$, and n_1 and n_2 are the parabolic related to the spherical quantum numbers n, l through $n = n_1 + n_2 + |m| + 1$). For atoms in electric fields, k is a good quantum number, and the simulations should remain valid as long as the magnetic field ($B = 0.5$–1 T) is relatively weak. These simulations allow us to evaluate the spread in velocity of the produced antihydrogen atoms, and to track these atoms through the 1 T magnet to the entrance of the Moiré deflectometer (figure 3). By ensuring that the electric-field gradient used to accelerate the produced Rydberg antihydrogen atoms is mainly axial, no significant change in their radial velocity distribution is expected. The divergence of the antihydrogen beam is thus defined by the longitudinal velocity (given by the Stark acceleration field strength and duration as well as the original velocity distribution) and the transverse velocity (given by the temperature of

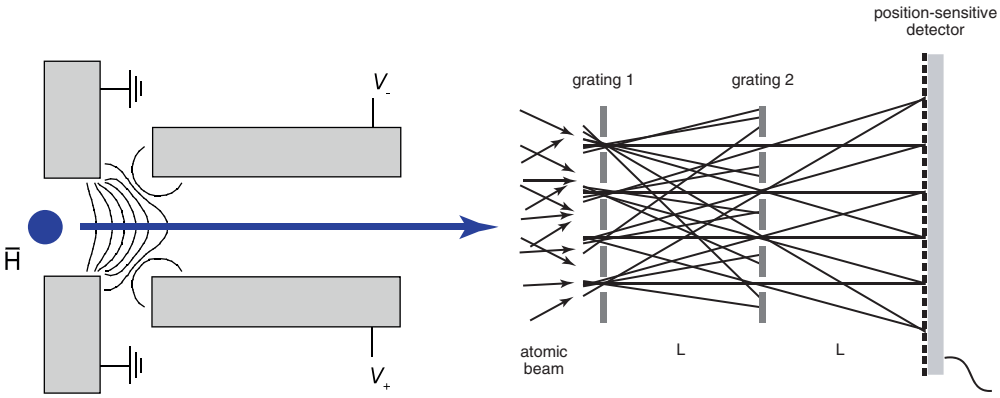

Figure 4. (Left) Sketch of the electrode configurations and resulting electric-field gradients used in Stark acceleration and deceleration of hydrogen atoms. (Right) Sketch of the principle of the Moiré deflectometer technique with two identical gratings and a position-sensitive detector.

the antiprotons prior to formation of antihydrogen, which is the dominant contribution to the antihydrogen velocity). The accelerating electric field will be applied for a time of the order of 70 μs. From simulations we expect an uncertainty of 10 μs on the beam starting time.

2.6. Antihydrogen beam through the Moiré deflectometer

In spite of its high sensitivity, a matter wave interferometer of the Mach–Zehnder type is poorly suited to first measurements with antihydrogen, mostly due to the very stringent limits it places on the beam divergence, but also due to expected decoherence effects through interactions between (anti-)matter waves and material gratings. Instead, AEGIS relies on a modified interferometer in which the grating period largely exceeds the de Broglie wavelength of the atoms, a so-called Moiré deflectometer. It is based on a design with which the local gravitational acceleration of a beam of argon atoms traveling at an average velocity of 750 m s^{-1} was measured to a relative precision of 2×10^{-4} [24]. The horizontally accelerated antihydrogen atoms (v∼500 m s^{-1}) propagate through the apparatus in the form of a broad beam until they enter the deflectometer, in which their free fall is measured. The deflectometer itself consists of two gratings and a third plane which records the impacting atoms (figure 4). The two gratings of a deflectometer function as a shadow mask, projecting a periodic pattern onto the third plane that corresponds to the gap and inter-gap geometry. This periodic structure along the vertical (y) coordinate has a period equal to the grating period (80 μm in AEGIS, although further optimization is being worked on). Antihydrogen atoms that do not pass through a grating gap annihilate, producing pions. Antihydrogen atoms that do pass through the gaps in the two planes will follow parabolic trajectories whose sagitta depends on the amount of time spent in the deflectometer, on average 2 ms, during which time the atom falls by 10 μm (for a grating distance of 40 cm). The periodic pattern (i.e. the antihydrogen impact points), whose edges are smeared by the transverse velocity of the transmitted antihydrogen atoms and the fact that the production source is extended, is thus shifted downward by an amount that depends on the velocity of the atoms. The vertical shift of the line pattern is $\delta_y = gt^2$, where t is the time of flight between the two gratings. The figure of merit is the fraction of accelerated antihydrogen atoms that reach and traverse the full Moiré deflectometer to impact the downstream high-resolution antihydrogen detector. This fraction is determined by the solid angle subtended by the detector, the divergence of the antihydrogen beam and the grating open fraction. As the transverse component of the velocity distribution is defined by the

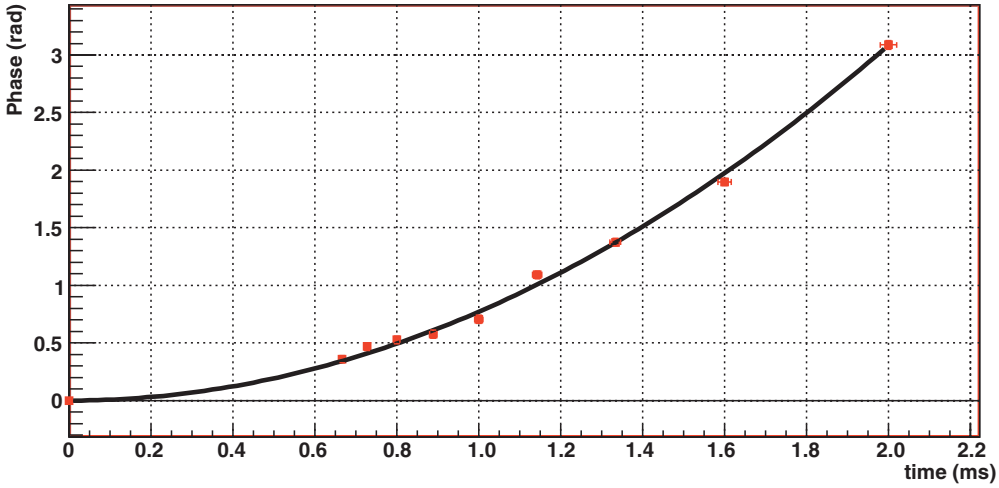

Figure 5. Phase shift as a function of the antihydrogen time of flight t between two gratings. Each point corresponds to 10^3 simulated antihydrogen atoms. A total of 10^5 atoms was generated and propagated through the Stark accelerator and Moiré interferometer. An impact vertex resolution of 10 μm was assumed. The precision in the determination of the phase at each point is influenced both by statistics and systematic effects; we estimate that the error on each point is ∼0.05 rad, although a full analysis has yet to be carried out. A quadratic fit to the plot of phase versus time of flight yields the local gravitational acceleration g.

antiproton temperature, it is desirable that this temperature be the lowest possible. By coupling the antiproton trapping electrodes to a 50 mK dilution refrigerator, different cooling techniques can be applied to attempt to reduce the temperature of the antiprotons from the current state of the art of a few K to a value of 100 mK. As the velocity scales with $T^{-1/2}$, while the solid angle scales as $(v_r/v_z)^2$, where v_r and v_z are the radial and axial velocity components, an increase by a factor of 10 of the temperature decreases the flux of antihydrogen atoms reaching the detector by the same factor. This purely geometrically defined flux is reduced by the open fraction of the two gratings of the deflectometer itself: the contrast of the periodic impact pattern in the plane of the detector is maximal in the case of an open fraction of 30%, resulting in a factor of 10 reduction in the flux. Our simulations have shown that in order to achieve a 1% measurement of g, 10^5 antihydrogen atoms with an initial temperature distribution (prior to acceleration) of 100 mK are required (a factor of 10 more for 1 K antiprotons). Assuming the production rate of section 2.4, and assuming that cooling of the antiprotons can be carried out during one AD duty cycle of 100 s, this corresponds to 10^4–10^5 AD cycles, i.e. several weeks to several months of experimental operation. Over such time scales, stability considerations are important; we will monitor the precise relative alignments of the gratings and the antihydrogen detector through a series of optical interferometers directly incorporated into these structures, allowing an offline correction of all measurements. On the other hand, the measurement of g is insensitive to variations in the flux of antihydrogen atoms. The value of g is extracted from the primary observables (time of flight t and vertical displacement of the fringe pattern δ_y, which can be transformed into a phase when normalized to the periodicity of the grating, as in figure 5).

3. Conclusion

The AEGIS experiment combines techniques, many of which are still under active development, from numerous fields to carry out a first measurement of the free fall of neutral

antimatter in the Earth's gravitational field using a pulsed cold beam of antihydrogen atoms. The precision of the gravity measurement is mainly limited by statistics, which in turn is mainly limited by the temperature of the produced antihydrogen atoms. Obtaining samples of anti-atoms at sub-K temperatures is therefore an important requirement for this experiment, although working with $\sim K$ antiprotons will allow a first measurement, albeit at a lower precision. Similarly, while many of the parameters in the experiment required to reach a 1% accuracy are challenging, somewhat lower efficiencies will not significantly affect the feasibility of the measurement, nor its accuracy. Gravity measurements with even higher precision as well as competitive CPT tests through spectroscopy will however necessitate the development of novel techniques to attain even colder antiproton and antihydrogen ensembles. Both physics topics and technical topics will be actively investigated over the coming years, leading up to the measurement of the gravitational interaction of antihydrogen. In the longer term, studies of antihydrogen (spectroscopy in flight, attempts at trapping Rydberg antihydrogen, attempts at cooling trapped Rydberg antihydrogen, attempts at carrying out spectroscopy of trapped Rydberg antihydrogen, e.g., via fluorescence or field ionization) will complement the improved gravitational measurement that can be carried out with a higher flux and colder antihydrogen. Cooling of trapped antihydrogen atoms in a field-free region outside the 1 T magnet then opens the door to much higher precision gravitational measurements and to high-precision spectroscopy, both of low-lying and of excited states.

References

[1] Drobychev G *et al* 2007 CERN-SPSC-2007-017, http://cdsweb.cern.ch/record/1037532
[2] Scherk J 1979 *Phys. Lett.* B **88** 265
Goldman T *et al* 1986 *Phys. Lett.* B **171** 217
Nieto M and Goldman T 1992 *Phys. Rep.* **205** 221–81
Barrow J and Scherrer R 2004 *Phys. Rev.* D **70** 103515
Alvarez C and Mann R 1997 *Phys. Rev.* D **55** 1732
[3] Jorgensen L V *et al* (ATHENA Collaboration) 2005 *Phys. Rev. Lett.* **95** 025002
[4] Gabrielse G *et al* (ATRAP Collaboration) 2002 *Phys. Lett.* B **548** 140
[5] Allison J *et al* 2006 *IEEE Trans. Nucl. Sci.* **53** 270–8
[6] Amoretti M *et al* 2004 *Nucl. Instrum. Methods Phys. Res.* A **518** 679
[7] Murphy T J and Surko C M 1992 *Phys. Rev.* A **46** 5696
[8] Gidley D W *et al* 2006 *Annu. Rev. Mater. Res.* **36** 49
[9] Mariazzi S, Salemi A and Brusa R S 2008 *Phys. Rev.* B **78** 085428
[10] Mariazzi S, Bettiotti P and Brusa R 2010 *Phys. Rev. Lett.* **104** 243401
[11] Ferragut R *et al* 2010 *J. Phys.: Conf. Ser.* **225** 012007
[12] Mariazzi S, Bettotti P, Larcheri S, Toniutti L and Brusa R S 2010 *Phys. Rev.* B **81** 235418
[13] Cialdi S *et al* 2011 *Nucl. Instrum. Methods Phys. Res.* B **269** 1527
[14] Castelli F, Boscoli I, Cialdi S and Comparat D 2008 *Phys. Rev.* A **78** 052512
[15] Cassidy D *et al* 2012 *Phys. Rev. Lett.* **108** 043401
[16] Hogan S 2011 private communication
[17] Mariazzi S, Toniutti L, Patel N and Brusa R 2008 *Appl. Surf. Sci.* **255** 191–3
[18] Andresen G B *et al* 2010 *Phys. Rev. Lett.* **105** 013003
[19] Gabrielse G *et al* 2011 *Phys. Rev. Lett.* **106** 073002
[20] Kellerbauer A and Walz J 2006 *New J. Phys.* **8** 45
[21] Warring U *et al* 2009 *Phys. Rev. Lett.* **102** 043001
[22] Fischer A *et al* 2010 *Phys. Rev. Lett.* **104** 073004
[23] Vliegen E and Merkt F 2006 *Phys. Rev. Lett.* **97** 033002
Vliegen E *et al* 2007 *Phys. Rev.* A **76** 023405
[24] Oberthaler M K *et al* 1996 *Phys. Rev.* A **54** 3165